J Med Dent Sci 2002; 49: 43–55

Original Article

Kinetic properties of tetrodotoxin-sensitive and tetrodotoxin-resistant sodium channel currents in neonatal rat trigeminal ganglion neurons

Masamichi Gotoh[1], Nobuhiro Noro[2] and Yoshinori Sahara[3]

Departments of 1) Restorative Sciences and 3) Maxillofacial Biology, Tokyo Medical and Dental University, Tokyo 113-8549, 2) Department of Discovery Biosciences, Research Division, GlaxoSmithKline K.K., Tsukuba, Ibaraki 300-4247, Japan

The kinetic properties of tetrodotoxin-sensitive (TTX-S) and tetrodotoxin-resistant (TTX-R) Na^+ channels in acutely dissociated neonatal rat trigeminal ganglion neurons were studied using whole-cell and cell-attached patch-clamp recordings. The time course of TTX-R currents was slower than that of TTX-S currents. Compared with TTX-S currents, TTX-R currents had more positive half-activation and half-inactivation voltages. TTX-R currents recovered from inactivation much faster than TTX-S currents. Cell-attached patch recordings showed that the slope conductance of single TTX-S and TTX-R channels was 14.6 pS and 7.8 pS, respectively. TTX-R channels had longer open-times and more dispersed latent-times than TTX-S channels. The convolution of the first latency distribution with the open-time distribution revealed that the slower time course of TTX-R currents is due to longer open-times and more dispersed latent-times of the TTX-R channels compared with those of the TTX-S channels. These findings suggest that TTX-R Na^+ channels in trigeminal ganglion neurons have similar kinetic property to brain TTX-S Na^+ channels, but not to structurally homologous cardiac Na^+ channels.

Corresponding Author: Masamichi Gotoh
Department of Restorative Sciences, Graduate School, Tokyo Medical and Dental University, 1-5-45, Yushima, Bunkyo-ku, Tokyo 113-8549, Japan. Phone: +81-35803-5494, FAX: +81-35803-5894, e-mail: m_gotoh@yahoo.co.jp
Present address of YS: Division of Biochemistry & Cellular Biology, National Institute of Neuroscience, National Center of Neurology and Psychiatry, Tokyo 187-8502, Japan.
Received December 28, 2001; Accepted March 4, 2002

Key words: Whole-cell recording; Single-channel recording; Convolution; RT-PCR.

Introduction

The voltage-gated Na^+ channel, a transmembrane glycoprotein responsible for the generation and propagation of action potentials in excitable cells, consists of a pore-forming α subunit and one or more auxiliary β-subunits. The α subunit has four homologous domains (I-IV), each with six predicted transmembrane segments (S1-6) joined by cytoplasmic and extracellular loops (for reviews see 1-2). The isolation of cDNA clones allows identification of a family of nine related α-subunit isoforms in mammals[3]. Voltage-dependent Na^+ channels of the brain and heart have structurally distinct α-subunit isoforms, and differ in sensitivity to tetrodotoxin (TTX). Na^+ channels in brain are blocked by nanomolar concentrations of TTX (TTX-sensitive, TTX-S), whereas TTX-resistant (TTX-R) Na^+ channels in heart are blocked by micromolar concentrations of TTX. Dorsal root ganglion (DRG) neurons express other family of Na^+ channel α subunits; one TTX-S Na^+ channel, called PN1[4,5] and two TTX-R Na^+ channels, SNS[6] or PN3[7] and NaN[8]. In all of these TTX-R Na^+ channel α subunits, TTX binds to a site in the SS2 domain, which forms part of the external loop that connects membrane spanning units S5 and S6. The kinetics of TTX-S Na^+ channels are faster than those of TTX-R Na^+ channels. Single-channel recordings have revealed that the TTX-S brain Na^+ channels open only briefly after waiting-times dispersed throughout the

decay phase[9], but that the slow inactivation of TTX-R cardiac Na^+ currents is a result of channel reopening[10]. Although homologous amino acid sequences between the cardiac and sensory ganglionic Na^+ channels are known, no explanation for the slow kinetics of TTX-R currents in sensory ganglion neurons has been reported. In the present study, we sought an explanation for the slow kinetics of TTX-R Na^+ currents in trigeminal ganglion neurons by comparing the kinetics of TTX-S channels with TTX-R channels using whole-cell and cell-attached patch-clamp recordings, and found that the slower time course of TTX-R currents is due to longer open-times and more dispersed latent-times of TTX-R channels than those of TTX-S channels.

Materials and Methods

Cell isolation and culture: Experiments were carried out following the NIH guidelines for the care and use of laboratory animals, and approved by the ethic committee of the Tokyo Medical and Dental University. Trigeminal ganglia were isolated after decapitation of halothane-anesthesized neonatal (2-8 days) Wistar rats. The detailed procedures is described elsewhere[11]. Briefly, dissected ganglia were incubated for 10-20 minutes at 37°C in Hank's solution (Gibco, Gaithersberg, MD, U.S.A.) containing 20 U/ml papain (Worthington Biochemical, Freehold, NJ, U.S.A.). Cells dissociated by trituration using a sterile Pasteur pipette were plated on poly-L-lysine pretreated 35 mm culture dishes. The plating medium contained Leibovitz's L-15 solution (Gibco), 10% fetal calf serum, penicillin-streptomycin (20 U/ml), 26 mM $NaHCO_3$ and 30 mM glucose. The cells were maintained at 37°C in a humidified atmosphere of 95% air-5% CO_2. Records were made between 2 and 10 hours after plating.

Recordings: Patch-clamp recordings were carried out at 20-24°C for whole-cell recordings and 12-16°C for single-channel recordings using an Axopatch 1-D amplifier (Axon Instruments, Foster City, CA, U.S.A.). Cells were visualized under phase contrast on an inverted microscope (Olympus IX-70, Tokyo, Japan). Pipettes for whole-cell recordings contained (mM): CsF 110, NaF 10, CsCl 40, $MgCl_2$ 2, ethylenglycol-bis (β-aminoethyl ether)-N,N,N′,N′-tetra acetic acid (EGTA) 2, and *N*-[2-hydroxyethyl] piperazine-*N*′-[2-ethanesulfonic acid] (HEPES) 10 (pH = 7.3); osmolarity was adjusted to 320 milliosmol/kg. The extracellular solution contained (mM): NaCl 20, tetraethyl ammonium chloride (TEA-Cl) 110, HEPES 10, $MgCl_2$ 2, $CaCl_2$ 1, glucose 10 (pH = 7.2, 325 milliosmol/kg). For drug application, an array of three quartz-glass tubes (400 μm in diameter, Polymicro Tech, Phoenix, AZ, U.S.A.) was connected to a gravity-fed reservoir and controlled by a three-way solenoid valve. TTX-R currents were recorded in the presence of 1 μM TTX. TTX was obtained from Sankyo (Tokyo, Japan). The pipette resistance of the whole-cell pipettes was 2-5 MΩ and the series resistance was 5-10 MΩ The series resistance was compensated ~60-80%. Leakage and capacitive currents were subtracted by using the P/-4 procedure of the pClamp (Axon Instruments). The junction potential between internal and external solutions was corrected. Pipettes for cell-attached patch recordings contained (mM): NaCl 150, CsCl or TEA-Cl 10, HEPES 10, $MgCl_2$ 1, $CaCl_2$ 1 (pH = 7.2, 325 milliosmol/kg). The extracellular solution for single-channel recording contained (mM): K-aspartate 150, CsCl 10, $MgCl_2$ 2, EGTA 10, and HEPES 10 (pH = 7.3); osmolarity was adjusted to 320 milliosmol/kg. A high K^+ solution effectively depolarizes the cell membrane outside the patch, and the resultant zero resting potential allows for complete control of the membrane potential[12,13]. The pipette resistance of the patch pipettes was 10-15 MΩ Capacitive and leakage currents were minimized by using sylgard-coated electrodes and electronic compensation.

Analysis: All Na^+ current records were filtered at 10 kHz (Bessel 8 pole, 48 dB/oct) and digitized using pClamp on a computer with a TL-1 DMA digital interface (Axon Instruments). The sampling rate was 20 kHz for whole-cell recordings and 50-100 kHz for single-channel recordings. The digitized records were analyzed using Axograph (Axon Instruments).

Analysis of whole- cell recordings; Na^+ conductance (G_{Na}) was calculated from the equation $G_{Na} = I_{Na}/(E-E_{Na})$, where I_{Na} is the peak amplitude of Na^+ current, E is the membrane potential, and E_{Na} is the reversal potential for sodium. The normalized conductance was fitted to the Boltzmann function $G/G_{max} = 1/1+exp\{(E_m-E_h)/k\}$, where E_m is the membrane potential, E_h is the half-activation potential, and k is the slope factor. The normalized peak current was fitted to the Boltzmann function $I/I_{max} = 1/1-exp\{(E_m-E_h)/k\}$, where E_m is the membrane potential, E_h is the half-inactivation potential, and k is the slope factor. The time course of recovery from inactivation was evaluated by normalizing the peak current evoked by second pulse (I_t) to the peak current evoked by first pulse (I_{max}) and

fitting to an exponential function of the time between the two pulses: $I_t / I_{max} = 1 - exp(-\tau / t)$, where t is the interval between the two pulses, and τ is the time constant of the recovery process. Tail currents were fitted to $I(t) = I_0 \, exp\,(-t/\tau)$, where τ is the time constant of exponential relaxation and I_0 is the current at $t = 0$.

Analysis of single-channel recordings; The amplitude and open time of the single-channel event were obtained from traces filtered at 2 kHz for TTX-R channel and 5 kHz for TTX-S channel using a digital Gaussian filter and channel events were selected manually. First latency distribution was obtained by determining the latency between the beginning of each test pulse and the first channel event in the record. The latent-time histogram was fitted to the time derivative of the first latency cumulative probability function (LT_{cpf}) corrected for N channels [14]:

$$LT_{cpf} = 1 - \left(\frac{\rho_1}{\rho_1 - \rho_2} * e^{-\rho_2 t} - \frac{\rho_2}{\rho_1 - \rho_2} * e^{-\rho_1 t} \right)^N$$

, where ρ_1 and ρ_2 are inverse time constants. The probability of openings, $P_o(t)$, was calculated from the convolution of the first latency probability density function (PDF) for one channel with the probability that a channel is open at time t given that it was open at time 0 (i.e. beginning of the test pulse)[9]. The convolution was done numerically using the principle that convolution in the time domain is equivalent to multiplication in the Laplace domain. Laplace transforms of the expressions for the first latency PDF and open-time PDF were obtained and multiplied together. Curve fittings for the amplitude, open-time, and latent time histograms and convolution were made using a least-squares procedures implemented in Ky plot (version 3.0, http:// www.qualest.co.jp). Data are presented as mean±SEM.

Reverse transcriptase-polymerase chain reaction: Wistar rats were sacrificed on postnatal days 3, 6, 8, 10, 13 and 30, and total RNA was isolated from the trigeminal ganglion using a TRIZOL kit (Gibco) according to the manual provided by the manufacturer. First-strand cDNA was synthesized from 5 μg of rat RNA with reverse transcriptase in the presence of random hexamer (First-strand cDNA synthesis kit, Pharmacia). α subunits rbNa I-III, NaCh6, PN1, NaN/SNS2, PN3/SNS and β1-2 subunits were amplified by PCR with the following set primers (from 5′ to 3′): for rbNa I sense TGCAAGCTGTCCGCT GGTAATATAC, and antisense GTGATCGTGATATCAACCTGAAG (GenBank accession #X03638, 7385-7819 bp); for rbNa II sense ATGCTGCAGCTCTCATTCACACACG, and antisense TGGCTAAACAATACTGCAGGG (#X03639, 6807-7303 bp); for rbNa III sense ATCCGTGTCAACTGGACTCTAAGG, and antisense CTTGTGGACTTAGCAACATGGG (#Y00766, 6326-6732 bp); for NaCh6 sense ACCTGGGCAATGTCTCAGCGTTG, and antisense CACACATGTAACCTTCTGGAC (#L39018, 6462-6759 bp); for PN 1 sense CTGCTCTTCCTGGTCATGTTCATC, and antisense GTACATGTTCACCACAACCAG (#X82835, 4963-5280 bp); for NaN/SNS 2 sense CCCTGCTGCGCTCGGTGAAGAA, and antisense GACAAAGTAGATCCCAGAGG (#AF059030, 777-1168 bp); for PN 3/SNS sense GACGTGATTCACCAACTTCTCG, and antisense CCGACTCACAGGTATTGTCC (#X92184, 6328-6483 bp); for β-1 sense AGACCGAGGCAGTGTATG, and antisense CCCTCTTCACCCCATCAA (#M91808, 299-1272 bp); for β-2 sense TGAAAATGCACAGGGATGCC, and antisense CAAGCTTCCGGTTACTTGG (#U37026, 162-825 bp). Rat glyceraldehyde-3-phosphate dehydrogenase (GAPDH; Clontech, Palo Alto, CA, U.S.A.) was used as a control for PCR. PCR was performed for 30 cycles of amplification with denaturing at 95°C for 30 sec, annealing at 55°C for 1 min, and elongating at 72°C for 1 min at the end of the amplification in the presence of 1xVent Buffer (New England Biolab, Beverly, MA, U.S.A.), 0.5 mM dNTP, 0.5 mM of each primer and 1.25U of AmpliTaq polymerase (Perkin-Elmer, Norwalk, CT, U.S.A.). PCR products were separated by electrophoresis on 2.5% Metaphor agarose gel (FMC Bioproduct, Rockland, ME, U.S.A.) containing 0.5 μg/ml ethidium bromide.

Results

Na^+ channel subunits expressed in trigeminal ganglia

To find out which Na^+ channel subunits are expressed in trigeminal ganglia, we used the RT-PCR. RT-PCR products for all subunits- brain types (rbNa I-III and NaCh6), peripheral types (PN1, SNS/PN3 and NaN/SNS2), and β subunits (β1 and β2)- were detected (Figure 1). On postnatal day 3, the expression of all subunits was high, except that the only subunit seen at a barely detectable level was β1. After postnatal day 13, rbNa III, PN1, SNS/PN3, NaN/SNS2 and β2 were not expressed as strongly as they had been earlier, and

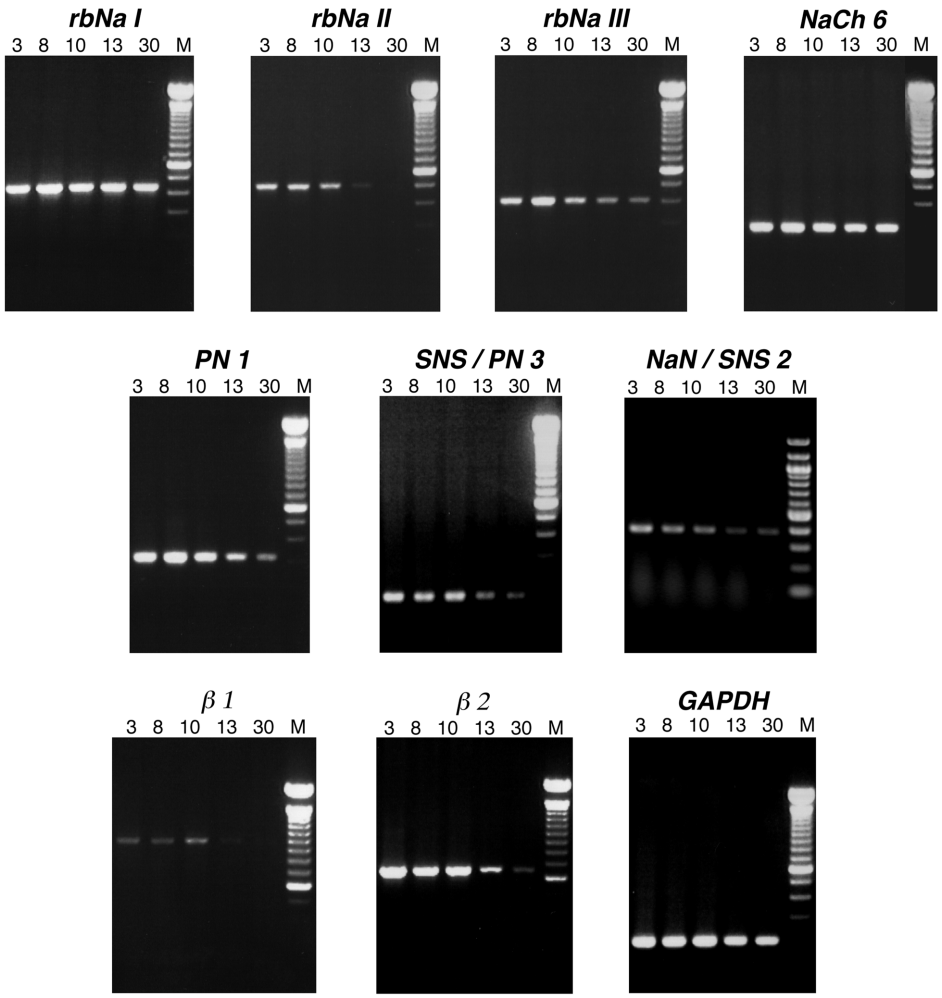

Figure 1. The expression of α subunits (rbNa I-III, NaCh6, PN1, SNS/PN3, NaN/SNS2) and β subunits (β1 and β2) transcripts in the trigeminal ganglion. RT-PCR primers were derived from specific sites for each subunit, and the predicted sizes of the PCR-generated fragments for the rbNa I-III, NaCh6, PN1, SNS/PN3, NaN/SNS2, β1 and β2 subunits were 435, 497, 407, 298, 318, 156, 392, 973 and 664 base pairs, respectively. Lanes marked 3,8,10,13 and 30 correspond to tissues obtained from rats on those postnatal days, and the lane marked M corresponds to a 100 bp ladder of markers. GAPDH was used as a control for the PCR.

rbNa II and β1 were barely detectable, whereas subunits rbNa I and NaCh6 were expressed uniformly throughout the 30 postnatal days. Thus, during the first few postnatal weeks, subunits for TTX-R Na^+ channels (rbNa III, SNS/PN3 and NaN/SNS2) appeared to be replaced by TTX-S channels (rbNa I and NaCh6) in trigeminal ganglia.

TTX-S and TTX-R Na^+ currents in whole-cell recordings

In trigeminal ganglion neurons, Na^+ currents having fast inactivation (Figure 2A) and those having slow inactivation (Figure 2D) were recorded. TTX (1.0 μM) blocked the former (TTX-S) but not the latter (TTX-R). The TTX-S current was likely to be present in larger trigeminal ganglion neurons and the TTX-R current was common in small to medium neurons (less than 30 μm in diameter of the cell body. The TTX-S current was encountered more frequently in adult and the TTX-R current was encountered more common in neonatal animals. TTX-S and TTX-R currents were frequently recorded in mixture. The ratio of TTX-S, TTX-R, and mixed Na^+ currents expressed in trigeminal ganglion neurons encountered in postnatal days 2-8 was 1:1:3 (n = 20), whereas the ratio on adults (2 month after birth) was 3:1:1 (n=10). Thus, the following data were

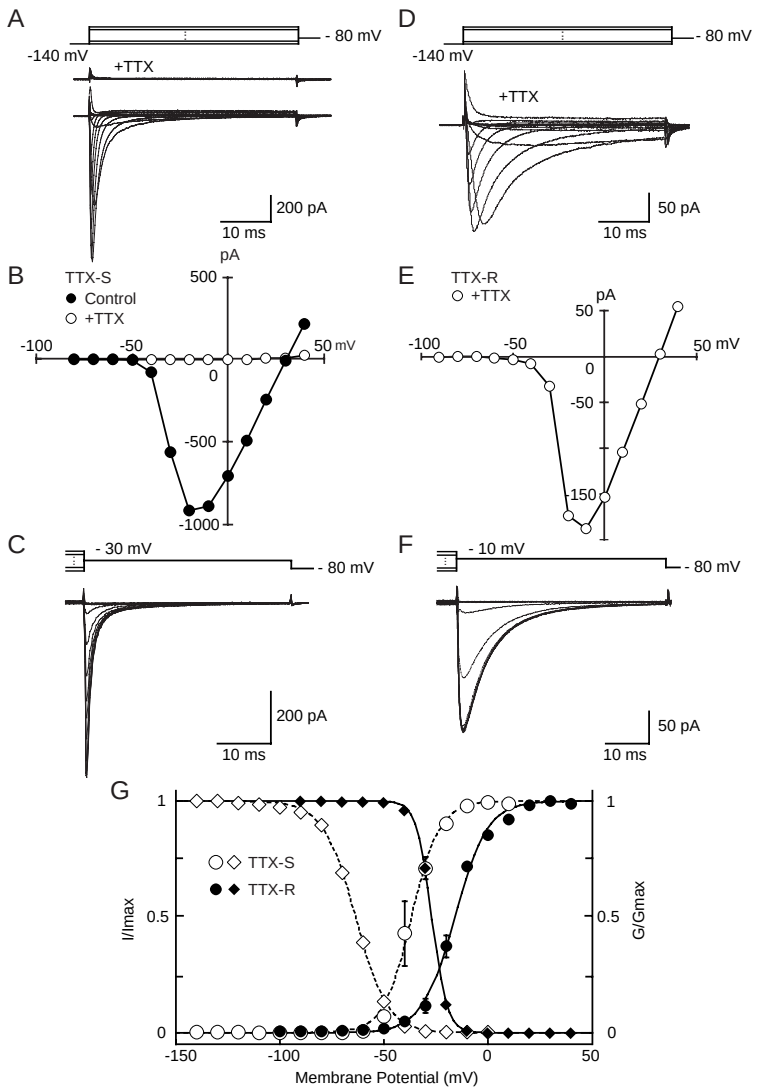

Figure 2. Voltage dependence of the activation and inactivation kinetics of TTX-S and TTX-R Na^+ currents in trigeminal ganglion neurons. A, TTX-S current traces measured with and without TTX (1 μM). D, TTX-R current traces in the presence of TTX (1 μM). Currents were elicited by 40 ms depolarizing steps in 10 mV increments. Each series of test pulses was preceded by a 400-1000 ms pulse to –140 mV. Na^+ currents were leak subtracted and membrane potential was held at –80 mV. B and E, I-V relationships for the peak Na^+ currents from A and D in the presence (open symbols) and absence (closed symbols) of TTX. C and F, Na^+ current traces after conditioning prepulses. The voltage dependence of inactivation was investigated by using a protocol, in which a cell was given a series of 400 ms prepulses ranging from –140 to +10 mV in 10 mV increments followed by a test voltage pulse of –10 mV for TTX-S currents (C) or 0 mV for TTX-R currents (F). Na^+ currents were not leak subtracted. G, normalized peak-conductance curves (circles) and steady-state inactivation curves (diamonds) of TTX-S and TTX-R currents. The peak current at a given test pulse (I) was normalized to I_{max} and plotted against prepulse voltages. The curves were obtained by fitting measured values to $G/G_{max} = 1/1+exp\{(E_m-E_h)/k\}$, where E_m is the membrane potential, E_h is the half-activation potential and k is the slope factor. The normalized peak current was fitted to the Boltzmann function $I/I_{max} = 1/1-exp\{(E_m-E_h)/k\}$, where E_h is the half-inactivation potential. Values plotted are means±S.E.M. for 4-6 cells.

obtained from neonatal rats (postnatal days 2-8). Figures 2B and 2E show the current-voltage (I-V) relationships of TTX-S and TTX-R currents. The reversal potentials of TTX-S currents (29.1 ± 0.81 mV, n=14) and TTX-R currents (28.6 ± 0.70 mV, n=19) were similar ($P > 0.05$, *t*-test), confirming that both currents were carried by Na^+. At all voltages examined, the TTX-R channels carried less current, and the maximum peak current for TTX-S channels was about ten times larger than that of TTX-R channels. In addition to the fast and slowly inactivated Na^+ current, a non-inactivated (persistent) Na^+ current[12,15] was also found in both TTX-S and TTX-R currents in trigeminal ganglion neurons (Figures 2A and 2D).

Steady-state activation and inactivation kinetics

TTX-S currents differed from those of TTX-R currents in the activation and inactivation kinetics (Figures 2C and 2F). In the G/G_{max} plot (Figure 2G), the half-activation voltage was –36.6±0.3 mV (n = 6) for the TTX-S current (open circles) and –16.0±0.4 mV (n = 8) for the TTX-R current (closed circles). In the steady-state inactivation, the half-inactivation voltage was –63.2 ± 0.2 mV (n = 5) for TTX-S currents (open diamonds) and –27.0±0.5 mV (n = 6) for TTX-R currents (closed diamonds). These results show that both the half-activation and half -inactivation potentials of TTX-R currents shift towards more depolarized values than those of TTX-S currents ($P<0.01$, *t*-test), which causes a region of overlap of the steady-state activation and inactivation curves.

The half-inactivation voltage for TTX-R currents in trigeminal neurons is similar to that in rat DRG cells (–25 mV England et al.[16] and –29 mV type B cells of Rush et al.[17], but see –45 mV Kostyuk et al.[18], Roy & Narahashi[19] and Ogata & Tatebayashi[20]). The inactivation curve for TTX-S currents in trigeminal ganglion neurons was fitted with a Boltzmann function, in contrast of DRG where neurons were fitted with a double Boltzmann function (half- inactivation values of –65 mV and –118 mV, Rush et al.[17]).

Recovery from inactivation

The time course of recovery from inactivation was studied using a double-pulse protocol. In these experiments, a trigeminal ganglion cell was voltage-clamped at –140 mV and 40 ms step pulses to –10 mV (TTX-S currents) or 0 mV (TTX-R currents) were given to activate and inactivate the current (Figures 3A and 3D). A second pulse followed the first one at increasing intervals, and the potential between the two pulses, recovery potential (V_r), ranged from –140 mV to 10 mV. Recovery from inactivation of TTX-S currents occurred faster at more negative recovery potentials. The time constant at V_r= –140 mV was 0.92 ± 0.04 ms (n = 4 cells) (closed squares in Figure 3B) and 15.02 ± 1.3 ms (n=3 cells) (open circles in Figure 3B) at –60 mV. At all voltages, the TTX-R currents recovered from inactivation faster than the TTX-S currents (Figures 3C and 3F; $P < 0.01$, *t*-test). The recovery time constant for TTX-R currents was 0.45±0.03 ms (n = 4 cells) at V_r= –130 mV (closed squares in Figure 3E), and 1.76± 0.23 ms (n = 3 cells) at –70 mV (open triangles in Figure 3E)

Tail currents of Na^+ channels

We next examined the tail currents of Na^+ channels. We activated a Na^+ current with either a 1.0 ms pulse to –20 mV for TTX-S currents or a 2.0 ms pulse to –10 mV for TTX-R currents, and then repolarized the membrane to –140 mV in 10 mV increments (Figures 4 A and 4C). Tail currents following a brief activating pulse could be well approximated by a single exponential function. At all voltages, the time constant of TTX-S currents was smaller than that of TTX-R currents (Figures 4 B and 4D).

Properties of single TTX-S and TTX-R Na^+ channels

Single-channel Na^+ currents were recorded in cell-attached patches in a high K^+ solution[12,13]. Trigeminal ganglion neurons contained high density of Na^+ channels such that most patches contained 4-20 Na^+ channels in a patch and no patches contained only one Na^+ channel. As shown in Figure 5A, TTX-S channel opening began with test pulses to –60 mV and consisted of early transient channel activity. With increasing depolarization, the brief initial openings became more synchronized. As shown in Figure 5C, TTX-R channel opening began with test pulses to –35 mV and channels stayed open much longer than TTX-S channels. The channel activity of TTX-R currents was recorded with pipette solutions added 10 nM TTX. Ensemble averages of single-channel currents (Figure 5B and 5D) revealed that the decay kinetics of the averaged currents in TTX-R channels (τ= 20.30 ms at –20 mV and τ= 3.73 ms at 0 mV) were slower than those of the currents in TTX-S channels (τ= 6.85 ms at –50 mV and τ=1.7 ms at –35 mV).

The mean amplitude of the single-channel current was determined by assembling a histogram of current magnitude, and these histograms were fitted by a Gaussian curve (Figures 6A and 6B). The conductance

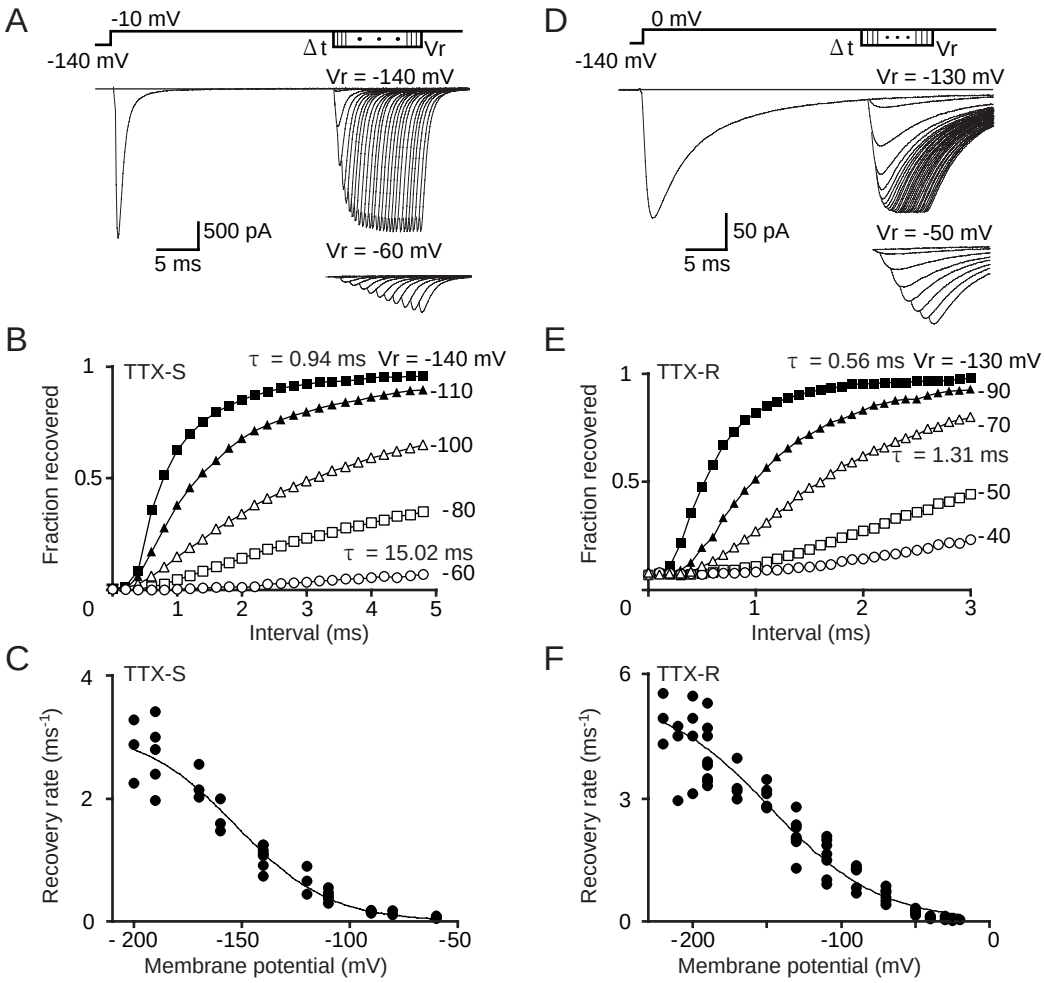

Figure 3. Recovery from inactivation of TTX-S and TTX-R currents. A, recovery from inactivation of TTX-S currents at different membrane potentials. The cell was held at –140 mV and pulsed twice to –10 mV for 40 ms with a gradually lengthened gap between the two pulses at recovery potential (V_r). The stimulus frequency was 0.1 Hz, and Na^+ currents were not leak subtracted. D, recovery from inactivation of TTX-R currents at different membrane potentials. The same protocol as in A except that dual pulse to 0 mV was used. B and E, the horizontal axis is the interval between two pulses, and the vertical axis is the extent of recovery. Normalized to the peak current evoked by the first pulse. The data points were fitted to $I_t / I_{max} = 1 - exp(-\tau / t)$, where t is the time between the two pulses, and τ is the time constant of the recovery process. The recovery potential is shown next to each curve. The data plotted in B was obtained from the TTX-S currents shown in A, and the data plotted in E was from the TTX-R currents shown in D. C and F, recovery rate (reciprocal of time constant) versus recovery potential. Data from 4-6 cells is plotted, and the continuous curves are least-squares fits to Boltzmann functions.

of TTX-S channels, calculated from current-voltage (*I-V*) plots of pooled data from 7 cells (Figure 6C), was 14.6 pS, whereas that of TTX-R channels was 7.8 pS. Both values are within the range of reported Na^+ single-channel conductances 7-17 pS[13,17,21,22].

As shown in Figures 5C, TTX-R channels tended to be open for long periods and openings were interrupted by brief periods of closure. TTX-S channels, in contrast, opened briefly and reopened infrequently (Figure 5A). Figure 7A1 shows that the histogram of the open-time of TTX-S channels at a test potential of –50 mV is fitted by a mono-exponential decay with a time constant of 0.29 ±0.05 ms (n = 5). The corresponding histogram for TTX-R channels is fitted by a mono-exponential decay with a time constant of 0.92±0.27 ms (n = 5) (Figure 7B1). The open-times of both TTX-R and TTX-S channels were independent of the test potentials. The latent-time histograms for TTX-S and TTX-R channels and the first latency distributions corrected for the presence of multiple channels[14] are plotted in

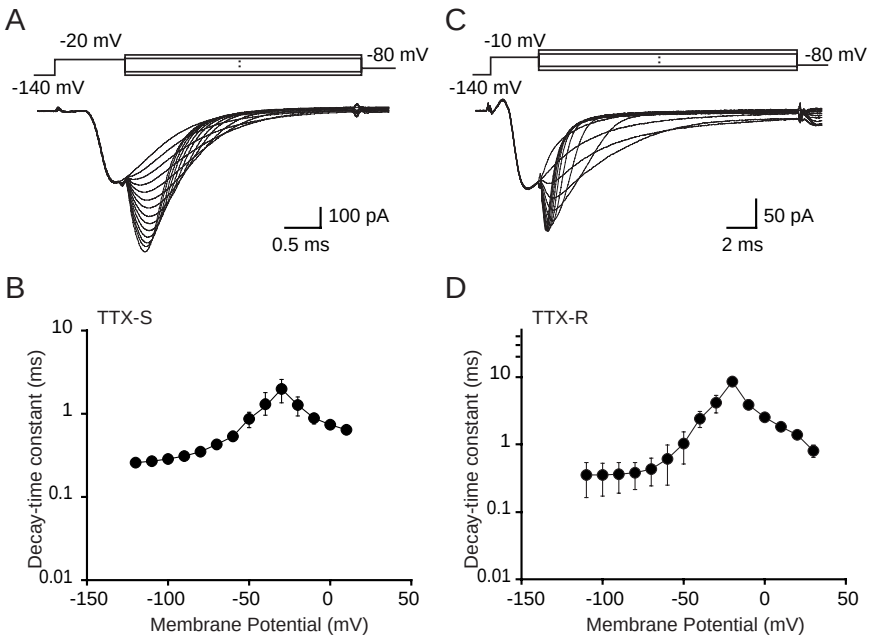

Figure 4. Tail currents of TTX-S and TTX-R currents. A, TTX-S current was activated by a 1 ms pulse to –20 mV and then repolarized in 10 mV increments. The holding potential was –140 mV. C, TTX-R current was activated by a 2 ms pulse to –10 mV and then repolarized in 10 mV increments. The holding potential was –140 mV. B and D, the vertical axis is the tail current time constant, and the horizontal axis is the voltage. The decay of tail current was fitted to a single exponential . Data from 4-6 cells is plotted.

Figures 7A2 and 7B2. Latent-times in TTX-R channels were longer than those in TTX-S channels ($P < 0.01$, *t*-test).

Kinetics differences of TTX-S and TTX-R Na^+ channels

In principle, the time course of the macroscopic Na^+ currents can be explained by the following three different single channel kinetics schemata; (1) the channel opens at an earlier time and remains open for a variable interval during the decay phase, (2) the channel opens only briefly with waiting-times dispersed throughout the decay phase, or (3) the channel opens and closes repetitively during the decay phase[23]. The first scheme predicts that the open duration distribution will have a mean comparable to the time constant of the decline in current. The open-time of TTX-R channels ($\tau = 1.04$ ms at –20 mV in Figure 6D) was too short to account for the time course of macroscopic inactivation ($\tau = 20.3$ ms at –20 mV in Figure 5D). The third scheme predicts that the first-latencies will be short, but that the open durations will be faster than the overall decay in current, and that a given channels will open a number of times during depolarization. In TTX-R Na^+ currents from trigeminal ganglion neurons, the number of openings did not far exceed the number of channels per patch. To see if the different first latency for TTX-S and TTX-R channels accounts for the different time courses of macroscopic inactivation, we convolved the first latency distribution with the open-time distribution. The close superposition of those convolutions and the average current from many traces, corresponding time courses of the probability of openings (the smooth curves and noisy curves in Figures 7A3 and 7B3), suggests that the latencies with which the TTX-R Na^+ currents open are dispersed enough to account for their slow kinetics.

Discussion

Kinetics of Na^+ channels in trigeminal ganglion neurons

The time course of TTX-R currents is slower than that of TTX-S currents in trigeminal ganglion neurons[24] as those in DRG neurons[17,18,19,25] and nodose ganglion neurons[26,27]. We have demonstrated that the slower time course of macroscopic TTX-R currents is

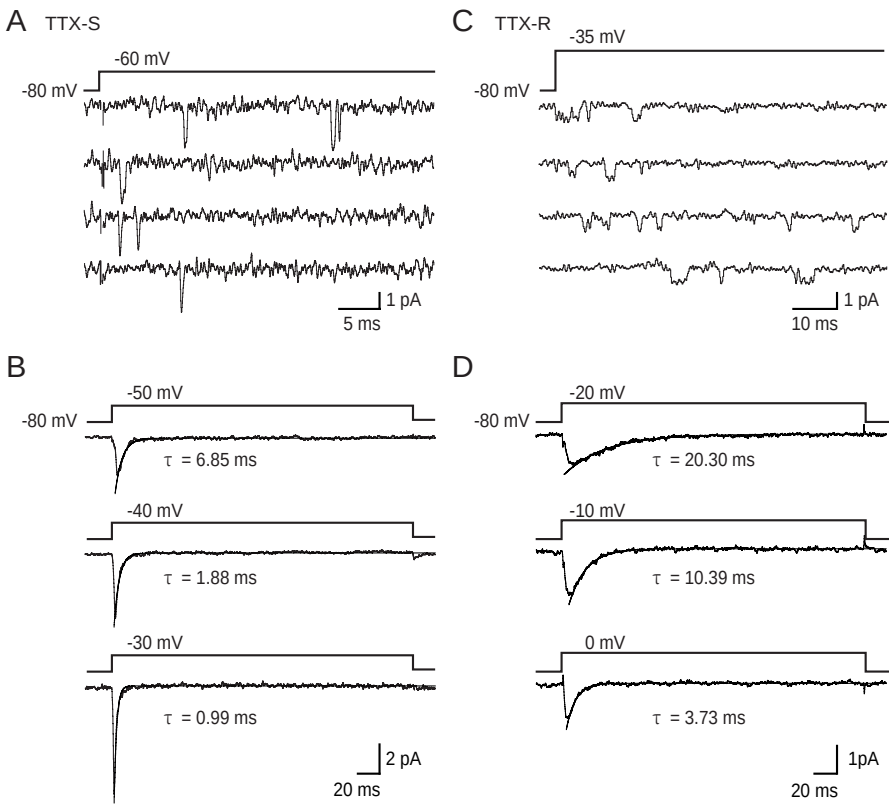

Figure 5. Single-channel currents of TTX-S and TTX-R channels in trigeminal ganglion neurons. A and C, traces of single-channel TTX-S (A) and TTX-R (C) Na^+ currents in cell-attached patches. Sample records were obtained during 40 ms test pulses delivered at 1 Hz to the potentials indicated. Records were digitally filtered at 5 kHz for TTX-S and at 2 kHz for TTX-R channels. B and D, reconstructions of macroscopic currents from single-channel recordings (averages of 30-100 records). The over-all time constants (τ) obtained by curve-fitting (smooth line) the decay phase were voltage dependent.

accounted for by the open-times and latent-times of the TTX-R channels being longer and more dispersed than those of the TTX-S channels. For cardiac TTX-R Na^+ currents, the latencies with which the TTX-R Na^+ currents open are not dispersed enough and the slow kinetics can be explained more appropriately by channel reopening[10]. It is interesting that TTX-R Na^+ channels in ganglion neurons and cardiac Na^+ channels use different kinetic mechanisms despite their structural homology, and that the kinetic mechanism followed by TTX-R Na^+ channels in trigeminal ganglion neurons is similar to that followed by brain Na^+ channels[9]. Identifying the sequences responsible for differences in function could be useful for understanding the structural basis for functional differences. The molecular basis of Na^+ channel inactivation in TTX-S currents has been clarified in a variety of excitable membranes[28,29,30]. Three amino acids (isoleucine, phenylalanin and methionine, IFM) in the short cytoplasmic loop connecting transmembrane domains III and IV have been demonstrated to be essential for fast inactivation[30,31,32]. Amino acid residues that are proposed inactivation particles are well conserved in both TTX-S and TTX-R channel subunits. α-scorpion toxins and sea anemone toxins (ATX) have also been known to affect the slowing of Na^+ channel inactivation. These neurotoxins have been shown to bind at the extracellular end of IVS4 and could slow or block the translocation, preventing inactivation and gating charge immobilization[33,34]. TTX-R currents in trigeminal ganglion neurons, however, are not sensitive to ATX[35]. Furthermore, auxiliary subunits have been shown to affect the time course of activation and inactivation gating processes. The effects of β1 subunits on the time courses of activation and inactivation, and perhaps on the voltage-dependence of inactivation, appear to

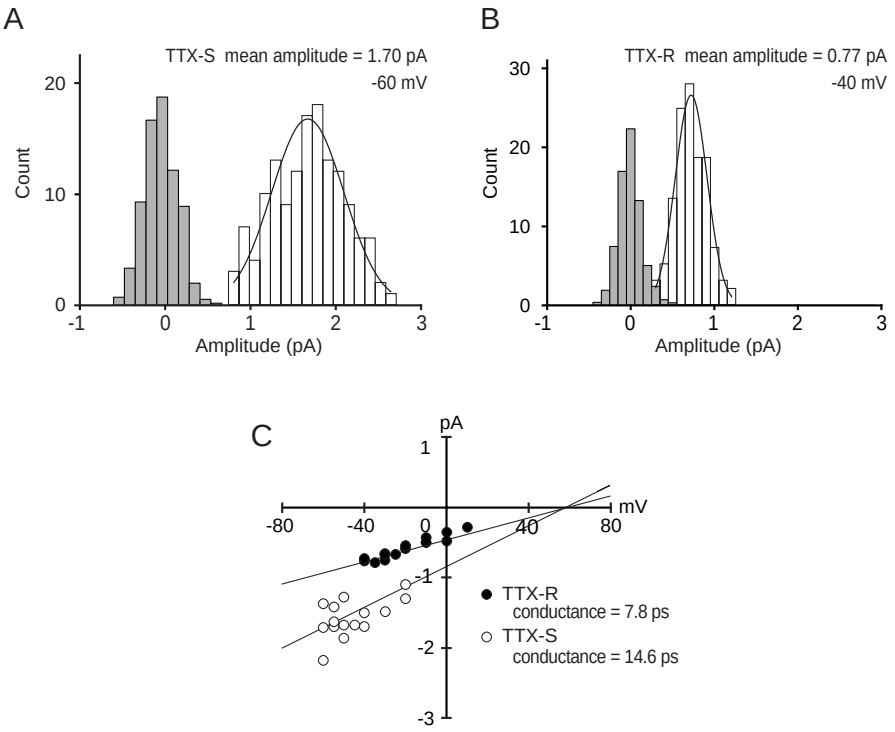

Figure 6. Single-channel conductance of the TTX-S and TTX-R channels in trigeminal ganglion neurons. A and B, single-channel amplitude histograms of data obtained when the test potential was –60 mV (n = 142 events) for TTX-S channels and –40 mV (n = 165 events) for TTX-R channels. The holding potential was –80 mV. Baseline noise is shown by shaded columns. At each test potentials, mean single-channel amplitude was determined as the mean amplitude of the Gaussian fit: 1.70±0.40 pA for the TTX-S channels and 0.77±0.21 pA for the TTX-R channels. The bin width is 0.12 pA in A and 0.1 pA in B. C, mean single-channel amplitude versus test potential. Plotted data for TTX-S channels is pooled data from 7 cells and data for TTX-R channels is 5 cells. Single-channel conductances calculated from the slope of the regression lines were 14.6 pS for the TTX-S channel and 7.8 pS for the TTX-R channel.

result from a shift from the slow to the rapid gating mode[36]. β1 was at a barely detectable level in the trigeminal ganglion. Thus, the molecular mechanism underlying the difference in the Na^+ channel inactivation between TTX-S and TTX-R currents remains to be seen.

Function of Na^+ channels and developmental changes of subunit expression in trigeminal ganglion neurons

Sodium channels play a crucial role in the generation and conduction of action potentials. In primary afferent nociceptors, Na^+ channels are thought to be involved in normal transduction processes as well as in modulatory processes[37]. TTX-R currents are observed in a subpopulation of neurons with nociceptor properties[38]. It has been suggested that Na^+ channels blocking agents are effective for the treatment of hyperalgesis and pain (for a review see 37). The contribution of TTX-R sodium channels (SNS or PN3) to the primary afferent nociceptor sensitization induced by inflammatory mediator has been strongly suggested[39,40]. On the other hand, studies in SNS-null transgenic mice have also demonstrated that SNS produces slowly inactivating TTX-R currents, and NaN produces persistent sodium currents[41]. In trigeminal ganglion neurons, there is a wider region of overlap of steady-state activation and inactivation curves for the TTX-R Na^+ channel, and both SNS/PN3 and NaN/SNS2 subunits were expressed, suggesting that increased overlap between inactivation and activation curves could augment the amplitude of the slow depolarizing potential and accelerate a long train of action potentials.

We have also shown that in the trigeminal ganglion, the Na^+ channel subunits rbNa I and NaCh6 were expressed throughout development, whereas other

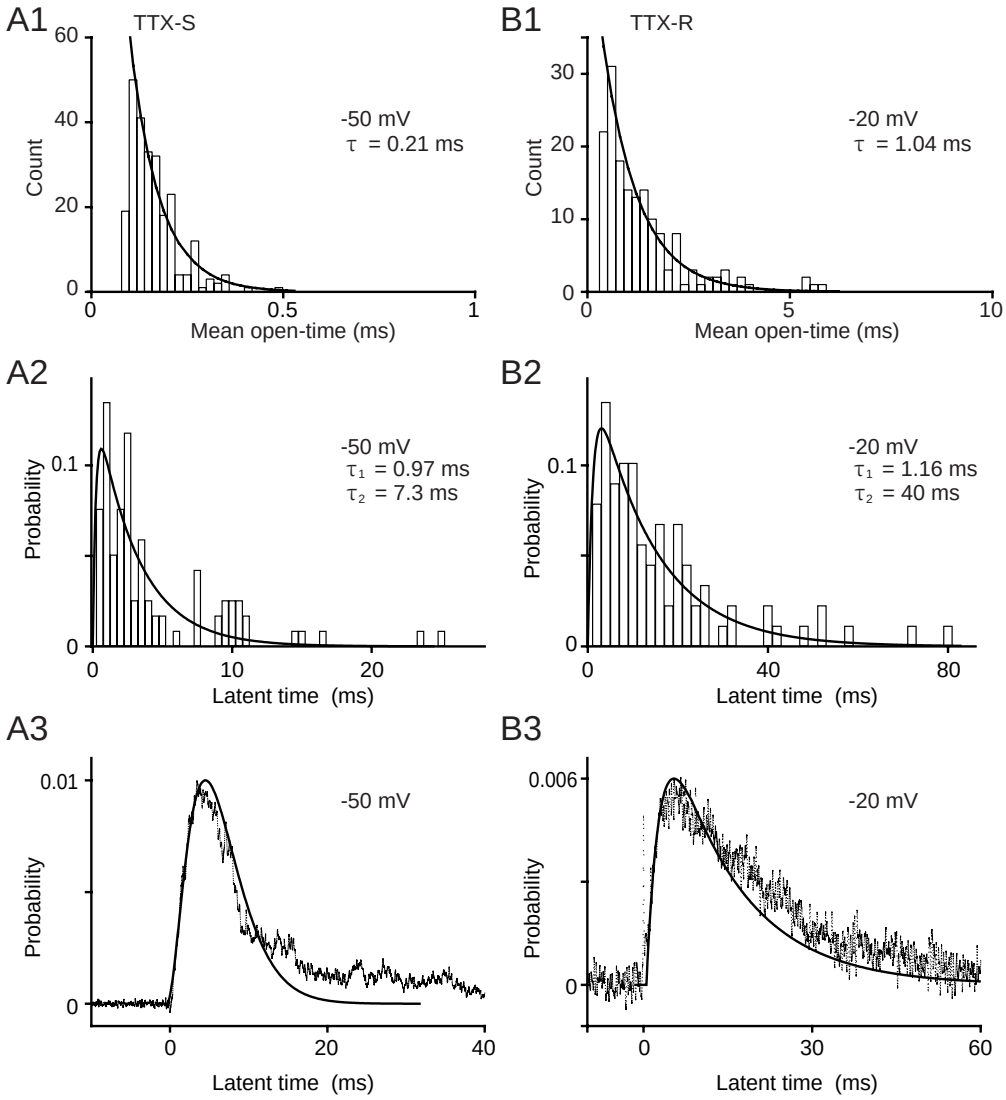

Figure 7. Open-time and latent-time distributions of TTX-S and TTX-R channels in trigeminal ganglion neurons. The open-time data (A1 and B1) and latent-time data (A2 and B2) at –50 mV for the TTX-S channels and –20 mV for the TTX-R channels from a holding potentials –80 mV. When the open-time frequency histograms in A1 (n = 479 events) and B1 (n = 183 events) were fitted to monoexponential distributions by using a least-squares algorithm, the time constant was 0.21 ms for the TTX-S channels and 1.04 ms for the TTX-R channels. When the latent-times frequency histograms in A2 (n = 95 events) and B2 (n = 89 events) were fitted to the time derivative of the first latency cumulative probability function (cpf) corrected for channel numbers, the time constants were 0.97 ms and 7.3 ms (N = 6 channels) for the TTX-S channels and 1.16 ms and 40 ms (N = 4 channels) for the TTX-R channels. A3 and B3, the shape of the convolution of the open-time and first latency distributions (smooth curves) are similar to the shapes of the corresponding time courses of the probability of opening ($P_o(t)$, noisy traces). The convolution predicts $P_o(t)$ reasonably well when channels open with dispersed latencies as in the Aldrich et al.[9]

subunits (rbNa III, PN1, SNS/PN3 and NaN/SNS 2) were expressed more predominantly in earlier postnatal stages. The changing pattern during development is clearly different from the CNS, where mRNA for type II sodium channel is expressed throughout all developmental stages, mRNA for brain type I sodium channel is predominant at late postnatal stages, and mRNA for the brain type III sodium channel expresses predominantly in fetal and early postnatal stages[42]. The differential subunit expression in the trigeminal ganglion may correlate with that of TTX-R Na^+ channels in the trigeminal ganglion which are gradually replaced by

TTX-S channels over the early postnatal period as they are in the DRG[19]. Around postnatal days 4-11, the innervation of the trigeminal nerve takes on the adult pattern with the appearance of hair follicules in the dermis[43]. During the first 3 postnatal weeks, about one-half of the cells in DRG neurons lose TrkA, where seventy to eighty percent of small DRG neurons with unmyelinated axons and most neurons projecting to lamina I and II of the superficial dorsal horn[44]. Considering that SA1 and D-hair mechanoreceptors as well as small DRG neurons require neurotrophin NGF for embryonic survival[43], NGF is involved in regulating the expression of both TTX-S and TTX-R Na^+ channels in sensory neurons. In fact, when access to the source of NGF is interrupted, as in the case of axotomy, TTX-R Na^+ channels decreases whereas that of brain type III increases and an increase in the density of TTX-S channels is observed[38]. Furthermore, the β2 subunits can be the rate-limiting step in the appearance of the adult level of mature Na^+ channel complexes. β2 subunits appear with α subunits during early neural development, and increased expression is observed during rapid neuronal growth and differentiation[45]. The striking similarity of the amino acid sequences of the β2 subunit and neuronal cell surface adhesion proteins contactin/F3 suggests that the β2 subunit may participate in cell-cell or cell-matrix interactions in development.

Acknowledgements

We thank Takayuki Gotoh and Misuzu Nakajima for helping with the experiments, and Gary Bennett, Tomoyuki Takahashi and Hideaki Suda for reading the manuscript.

References

1. Marban E, Yamagishi T, Tomaselli GF. Structure and function of voltage-gated sodium channels. *J Physio*l 1998: 508, 647-657.
2. Catterall WA. From ionic currents to molecular mechanisms: the structure and function of voltage-gated sodium channels. *Neuron* 2000; 26: 13-25.
3. Goldin AL. Resurgence of sodium channel research. *Annu Rev Physiol* 2001; 63: 871-894.
4. Toledo-Aral JJ, Moss BL, He Z-J. et al. Identification of PN1, a predominant voltage-dependent sodium channel expressed principally in peripheral neurons. *Proc Natl Acad Sci USA* 1997; 94: 1527-1532.
5. Sangameswaran L, Fish LM, Koch BD. et al. A novel tetrodotoxin-sensitive, voltage-gated sodium channel expressed in rat and human dorsal root ganglia. *J Biol Chem* 1997; 272: 14805-14809.
6. Akopian AN, Sivilotti L, Wood JN. A tetrodotoxin-resistant voltage-gated sodium channel expressed by sensory neurons. *Nature* 1996; 379: 257-262.
7. Sangameswaran L, Delgado SG, Fish LM. et al. Structure and function of a novel voltage-gated, tetrodotoxin-resistant sodium channel specific to sensory neurons. *J Biol Chem* 1996; 271: 5953-5956.
8. Dib-Hajj SD, Tyrrell L, Black JA. et al. NaN, a novel voltage-gated Na channel, is expressed preferentially in peripheral sensory neurons and down-regulated after axotomy. *Proc Natl Acad Sci USA* 1998; 95: 8963-8968.
9. Aldrich RW, Corey DP, Stevens CF. A reinterpretation of mammalian sodium channel gating based on single channel recording. *Nature* 1983; 306: 436-441.
10. Kirsch GE, Brown AM. Kinetic properties of single sodium channels in rat heart and rat brain. *J Gen Physiol* 1989; 93: 85-99.
11. Sahara Y, Noro N, Iida Y. et al. Glutamate receptor subunits GluR5 and KA-2 are coexpressed in rat trigeminal ganglion neurons. *J Neurosci* 1997; 17: 6611-6620.
12. Alzheimer C, Schwindt PC, Crill WE. Modal gating of Na^+ channels as a mechanism of persistent Na^+ current in pyramidal neurons from rat and cat sensorimotor cortex. *J Neurosci.*1993; 13: 660-673.
13. Roy ML, Reuveny E, Narahashi T. Single-channel analysis of tetrodotoxin-sensitive and tetrodotoxin-resistant sodium channels in rat dorsal root ganglion neurons. *Brain Res* 1994; 650: 341-346.
14. Patlak J, Horn R. Effect of *N*-bromoacetamide on single sodium channel currents in excised membrane patches. *J Gen Physiol* 1982; 79: 333-351.
15. Llinás R, Sugimori M. Electrophysiological properties of *in vitro* Purkinje cell dendrites in mammalian cerebellar slices. *J Physiol* 1980; 305: 197-213.
16. England S, Bevan S, Docherty RJ. PGE_2 modulates the tetrodotoxin-resistant sodium current in neonatal rat dorsal root ganglion neurones via the cyclic AMP-protein kinase A cascade. *J Physiol* 1996; 495: 429-440.
17. Rush AM, Bräu ME, Elliott AA. et al. Electrophysiological properties of sodium current subtypes in small cells from adult rat dorsal root ganglia. *J Physiol* 1998; 511: 771-789.
18. Kostyuk PG, Veselovsky NS, Tsyndrenko AY. Ionic currents in the somatic membrane of rat dorsal root ganglion neurons I. sodium currents. *Neuroscience* 1981; 6: 2423-2430.
19. Roy ML, Narahashi T. Differential properties of tetrodotoxin-sensitive and tetrodotoxin-resistant sodium channels in rat dorsal root ganglion neurons. *J Neurosci* 1992; 12: 2104-2111.
20. Ogata N, Tatebayashi H. Kinetic analysis of two types of Na^+ channels in rat dorsal root ganglia. *J Physiol* 1993; 466: 9-37.
21. Campbell DT. Single-channel current/voltage relationships of two kinds of Na^+ channel in vertebrate sensory neurons. *Pflüger Arch* 1993; 423: 492-496.
22. Motomura H, Fujikawa S, Tashiro N. et al. Single-channel analysis of two types of Na^+ currents in rat dorsal root ganglia. *Pflügers Arch* 1995; 431: 221-229.
23. Aldrich RW. Voltage-dependent gating of sodium channels: towards an integrated approach. *Trends Neurosci* 1986; 9: 82-86.
24. Kim H-C, Chung M-K. Voltage-dependent sodium and calcium currents in acutely isolated adult rat trigeminal root ganglion neurons. *J Neurophysiol* 1999; 81: 1123-1134.
25. Elliott AA, Elliott JR. Characterization of TTX-sensitive and TTX-resistant sodium currents in small cells from adult rat dor-

sal root ganglia. *J Physiol* 1993; 463: 39-56.
26. Bossu J-L, Feltz A. Patch-clamp study of the tetrodotoxin-resistant sodium current in group C sensory neurones. *Neurosci Lett* 1984; 51: 241-246.
27. Ikeda SR, Schofield GG. Tetrodotoxin-resistant sodium current of rat nodose neurones: monovalent cation selectivity and divalent cation block. *J Physiol* 1987; 389: 255-270.
28. Bezanilla F, Armstrong CM. Inactivation of the sodium channel. I. Sodium current experiments. *J Gen Physiol* 1977; 70: 549-566.
29. Armstrong CM, Bezanilla F. Inactivation of the sodium channel. II. Gating current experiments. *J Gen Physiol* 1977; 70: 567-590.
30. Stuhmer W, Conti F, Suzuki H. et al. Structural parts involved in activation and inactivation of the sodium channel. *Nature* 1989; 339: 597-603.
31. Vassilev PM, Scheuer T, Catterall WA. Identification of an intracellular peptide segment involved in sodium channel inactivation. *Science* 1988; 241: 1658-1661.
32. West JW, Scheuer T, Maechler L. et al. Efficient expression of rat brain type IIA Na^+ channel α subunits in a somatic cell line. *Neuron* 1992; 8: 59-70.
33. Rogers JC, Qu Y, Tanada TN. et al. Molecular determinants of high affinity binding of α-scorpion toxin and sea anemone toxin in the S3-S4 extracellular loop in domain IV of the Na^+ channel α subunit. *J Biol Chem* 1996; 271: 15950-15962.
34. Cestèle S, Qu Y, Rogers JC. et al. Voltage sensor-trapping: enhanced activation of sodium channels by β-scorpion toxin bound to the S3-S4 loop in domain II. *Neuron* 1998; 21: 919-931.
35. Sahara Y, Gotoh M, Konno K. et al. A new class of neurotoxin from wasp venom slows inactivation of sodium current. *Eur J Neurosci* 2000; 12: 1961-1970.
36. Patton DE, Isom LL, Caterall WA, et al. The adult rat brain β1 subunit modifies activation and inactivation gating of multiple sodium channel α subunits. *J Biol Chem* 1994; 269: 17649-17655.
37. McCleskey EW, Gold MS. Ion channels of nociception. *Annu Rev Physiol* 1999; 61: 835-856.
38. Cummins TR, Waxman SG. Downregulation of tetrodotoxin-resistant sodium currents and upregulation of a rapidly repriming tetrodotoxin-sensitive sodium current in small spinal sensory neurons after nerve injury. *J Neurosci* 1997; 17: 3503-3514.
39. Akopian AN, Souslova V, England S. et al. The tetrodotoxin-resistant sodium channel SNS has a specialized function in pain pathways. *Nat Neurosci* 1999; 2: 541-548.
40. Gold MS, Reichling DB, Shuster MJ. et al. Hyperalgesic agents increase a tetrodotoxin-resistant Na^+ current in nociceptors. *Proc Natl Acad Sci USA* 1996; 93: 1108-1112.
41. Cummins TR, Dib-Hajj SD, Black JA. et al. A novel persistent tetrodotoxin-resistant sodium current in SNS-null and wild-type small primary sensory neurons. *J Neurosci* 1999; 19: RC43 (1-6).
42. Catterall WA. Cellular and molecular biology of voltage-gated sodium channels. *Physiol Rev* 1992; 72: S15-48.
43. Lewin GR, Mendell LM. Nerve growth factor and nociception. *Trends Neurosci* 1993; 16: 353-359.
44. Molliver DC, Snider WD. Nerve growth factor receptor TrkA is down-regulated during postnatal development by a subset of dorsal root ganglion neurons. *J Comp Neurol* 1997; 381: 428-438.
45. Isom LL, Ragsdale DS, De Jongh KS. et al. Structure and function of the β2 subunit of brain sodium channels, a transmembrane glycoprotein with a CAM motif. *Cell* 1995; 83: 433-442.